



# CHORUS

This is the accepted manuscript made available via CHORUS. The article has been published as:

## First Measurements of Deuterium-Tritium and Deuterium-Deuterium Fusion Reaction Yields in Ignition-Scalable Direct-Drive Implosions

C. J. Forrest, P. B. Radha, J. P. Knauer, V. Yu. Glebov, V. N. Goncharov, S. P. Regan, M. J. Rosenberg, T. C. Sangster, W. T. Shmayda, C. Stoeckl, and M. Gatu Johnson

Phys. Rev. Lett. **118**, 095002 — Published 3 March 2017

DOI: [10.1103/PhysRevLett.118.095002](https://doi.org/10.1103/PhysRevLett.118.095002)

# First Measurements of Deuterium–Tritium and Deuterium–Deuterium Fusion- Reaction Yields in Ignition-Scalable Direct-Drive Implosions

C. J. Forrest,<sup>1</sup> P. B. Radha,<sup>1</sup> J. P. Knauer,<sup>1</sup> V. N. Goncharov,<sup>1</sup> V. Yu. Glebov,<sup>1</sup> S. P.  
Regan,<sup>1</sup> M. J. Rosenberg,<sup>1</sup> T.C. Sangster,<sup>1</sup> W. T. Shmayda,<sup>1</sup> C. Stoeckl,<sup>1</sup>  
and M. Gatu Johnson<sup>2</sup>

<sup>1</sup>Laboratory for Laser Energetics, University of Rochester, New York 14623, USA

<sup>2</sup>Massachusetts Institute of Technology, Cambridge, MA 02139, USA

The deuterium–deuterium (D–D) and deuterium–tritium (D–T) neutron yield ratio in cryogenic inertial confinement fusion (ICF) experiments are used to examine multifluid effects, traditionally not included in ICF modeling. This ratio has been measured for ignition-scalable direct-drive cryogenic DT implosions at the Omega Laser Facility [T. R. Boehly *et al.*, *Opt. Commun.* **133**, 495 (1997)] using a high-dynamic-range neutron time-of-flight spectrometer. The experimentally inferred yield ratio is consistent with both the calculated values of the nuclear reaction rates and the measured pre-shot target-fuel composition. These observations indicate that the physical mechanisms that have been proposed to alter the fuel composition, such as species separation of the hydrogen isotopes [D. T. Casey *et al.*, *Phys. Rev. Lett.* **108**, 075002 (2012)], are not significant during the period of peak neutron production in ignition-scalable cryogenic direct-drive DT implosions.

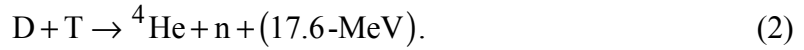
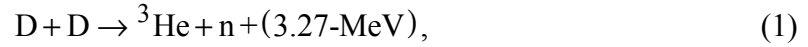
In direct-drive inertial confinement fusion (ICF) ignition designs, a cryogenic deuterium–tritium (DT) shell surrounding a vapor and encased in a thin-plastic (CH) or deuterated plastic (CD) ablator ( $<10 \mu\text{m}$ ) is symmetrically heated with nominally identical laser beams. In most designs, laser ablation launches one or multiple shocks through the converging shell and into the vapor region. The shock-transit stage of the implosion is followed by a deceleration phase, where the kinetic energy of the converging shell is converted to the internal energy of the hot spot. Thermonuclear fusion reactions are initiated in both the shock phase and the compression phase once sufficiently high temperatures and densities are reached [1]. To achieve conditions relevant for ignition implosion designs, the hot-spot size must exceed the mean free path of fusing ions. This requirement is essential to maximize the energy deposition of the alpha particle in the hot spot.

Previous experiments have reported anomalous  $Y_{\text{DT}}/Y_{\text{DD}}$  values (different by as much as a factor of 4) with the measured pre-shot fuel composition and experimentally inferred ion temperatures in room-temperature implosions [2]. Several studies suggest that species separation of the hydrogen isotope resulting from multifluid effects [3,4] are likely responsible for the observed discrepancies in the yield ratios. These class of implosions, for example, exploding pushers that use thin-glass ( $\sim 3\text{-}\mu\text{m}$   $\text{SiO}_2$ ) or thin-CH ( $<16\text{-}\mu\text{m}$ ) shells are, however, characterized by fusion reactions that occur predominantly during the shock phase at very high temperatures ( $\geq 10 \text{ keV}$ ) and relatively low densities ( $\leq 10 \text{ mg/cm}^3$ ). The mean free path for  $90^\circ$  deflection is given by  $\lambda_{\text{ii}} \sim T_i^2 / Z_i^2 Z^2 \rho$  [5] for ions of charge  $Z_i$ , average ion temperature  $T_i$ , ion charge  $Z$ , and density  $\rho$ . Conditions during the shock phase result in large mean-free-path lengths of the ions relative to the size of the fusing-plasma

region (see Table I). These conditions are also typical of ignition-scalable direct-drive cryogenic implosions [6] during the shock phase; however, cryogenic targets differ from exploding pusher targets in two respects: First, most of the neutron yield in a cryogenic implosion occurs later in the implosion, during the compression phase, when the kinetic energy is converted to the internal energy of the hot spot. Simulations using the spherically symmetric hydrodynamic code *LILAC* [6] indicate that nearly 99% of the yield occurs in this compression phase. Second, compression yields occur at significantly higher densities ( $\geq 20$  g/cm<sup>3</sup>) and lower temperatures ( $\sim 3$  keV), leading to mean free paths of thermal ions that are much shorter than the hot-spot size. Nonlocal transport of energetic ions is therefore not expected to significantly influence yields during compression. Evidence of fuel species separation that persist into the compression phase, would suggest a reduction in the number of alpha particles produced from the dominant D–T fusion reactions. However, in ignition-scalable cryogenic implosions described in this Letter, measurements presented here give the first evidence that species separation does not persist from the shock phase and has an insignificant influence on the yield ratio into the compression phase in direct-drive D–T cryogenic implosions consisting of an equimolar mixture of deuterium–tritium [8].

Direct-drive ICF targets consisting of a deuterated plastic (ablator) shell with a 460- $\mu$ m outer radius are imploded at ignition-scalable, on-target laser intensity at a laser energy of  $\sim 25$  kJ [9]. The implosion velocity ( $V_{\text{imp}}$ , defined as the velocity of the compressing shell when the kinetic energy of the shell is at a maximum) ranged from  $3.5 \times 10^7$  cm/s to  $4 \times 10^7$  cm/s and adiabat ( $\alpha$ , defined as the ratio of the pressure to the Thomas–Fermi pressure at maximum shell density) ranged from 2.4 to 5. The average ion

temperature  $T_i$  in this class of implosion is varied by adjusting the implosion velocity,  $T_i \sim V_{\text{imp}}^{1.1}$ , which, in turn, is governed by the thickness of the cryogenic DT layers or the CH (CD) ablator. The capsule is filled by a permeation technique, where increasing pressure is applied to the outside of the shell, allowing the gas to diffuse inside. This procedure is performed at 300 K with a permeation time constant of the order of one minute. Fill rates for a typical cryogenically cooled target are  $\sim 1$  atm/min, which is carefully controlled to ensure the integrity of the shell is not compromised [10]. At the final fill pressure (between 400 and 800 atm) depending on the desired ice thickness, the capsule is cooled to a few mK below the triple point ( $\sim 19.8$  K), producing a DT ice layer ranging from 40 to 90  $\mu\text{m}$  in thickness. The primary nuclear-fusion reactions examined in this study are given by



The neutron yields are measured using the time-of-flight diagnostics (nTOF) positioned around the OMEGA target chamber. The fusion yield is given by  $Y_n^{\text{DT/DD}} = \int f_{\text{D}} f_{\text{D/T}} [\rho(\vec{r}, t)]^2 \langle \sigma v \rangle_{\text{DT/DD}} dr^3 dt / (1 + \delta_{\text{DD}}) \bar{m}^2$ , where  $f_{\text{T}}$  and  $f_{\text{D}}$  are the atomic fractions of the reactants,  $\rho$  is the fuel-mass density,  $\langle \sigma v \rangle$  is the Maxwellian-averaged reactivity for the D–T or D–D fusion reaction (which scales as  $\sim T_i^{3.7}$  for the D–T reaction and  $\sim T_i^{3.3}$  for the D–D reaction for the typical temperatures in OMEGA

implosions),  $T_i$  is the average ion temperature,  $\bar{m}$  is the average reactant mass, and the Kronecker delta ( $\delta_{DD}$ ) is required to account for the double counting of the identical deuterium–deuterium reaction.

The primary D–T yields observed in cryogenic experiments are always lower relative to radiation–hydrodynamic codes that assume spherical symmetry and include the deposition of the laser energy through collisional absorption and account for laser–plasma interactions such as cross-beam energy transfer (CBET) [11]. These codes include nonlocal heat conduction [11] and multigroup diffusive radiative transport [12]. Several multidimensional effects that reduce the overall yield relative to these state-of-the-art spherically symmetric fluid codes have been proposed, including nonuniformity growth caused by beam-to-beam energy imbalance [13], on-target beam misalignment [14], single-laser-beam nonuniformity [14], and isolated defects on the target [15] that potentially reduce  $T_i$  and/or fuel density. All these mechanisms include only hydrodynamic effects and do not exhibit yield ratio anomalies. More recently, an extension to fluid codes has been proposed. Calculations that include plasma baro-diffusion [16,17], where hydrogen isotope species separation occurs during the shock phase into the hot spot because of gradients in pressure and temperature have been shown to influence the D–T and D–D fusion yields differently. Two phases of an ICF implosion have been analyzed using this model: the shock phase (when the shock is moving through the vapor toward the center of the capsule) followed by the rebound phase (outward-going shock). It was reported that during the shock phase up to 5% of the deuterium can leave the fuel volume for an equimolar mixture of deuterium–tritium. During the subsequent shock rebound phase, the barotropic diffusion rate decreases to zero and the ability for fuel to leave the volume is significantly reduced if

not eliminated. Since the D–D fusion and D–T fusion reactivity are well-known [18] and the composition of the fuel is measured prior to the implosion, the ratio of the neutron yields ratios ( $Y_{DT}/Y_{DD}$ ) from these reactions should follow a calculable trend with the measured ion temperature with the exclusion of diffusive effects. Table I summarizes the mass-fuel density ( $\rho$ ) and the key implosion parameters to calculate the ion–ion mean free path ( $\lambda_{ij}$ ) for the plasma conditions across the class of implosions discussed earlier in this Letter. The radius of the shell ( $R_{\text{shell}}$ ) is calculated from simulations for the different phases of the implosion.

As shown in Table I, the mean free path during the shock phase for the ions at the relevant average ion temperature approaches the radius of the shell. However, at this time, the vapor region is surrounded by a relatively cold ( $\sim 20$ -eV) and highly dense DT-fuel layer. The energetic and thermal ions that escape the vapor phase do not leave the target and instead are stopped in the cold dense DT shell. At peak neutron production, the mean free path is several orders of magnitude smaller ( $\sim 10^{-2}$ ) than the boundary of the cold-fuel shell.

Cryogenic implosions are additionally different from shock-driven implosions that have been studied previously since the shell material is also made of deuterium–tritium fuel. When the shell decelerates in the compression stage of any ICF implosion, the cold fuel ablates into the hot spot. Simulations using the code *LILAC* indicate that, in the case of cryogenic layered DT implosions, nearly  $5\times$  the mass of the original vapor [7] is injected into the hot spot through the ablation process and this is the primary source of the fusion neutrons during compression. Therefore, it would be expected that the ions that are stopped in the cold-fuel shell would be restored into the hot core during the

compression phase, compensating for any loss of particles that may have occurred earlier in the implosion.

For this analysis, the yields ( $Y_{DT}$  and  $Y_{DD}$ ) for the different reactions are measured along the same diagnostic line of sight using a high-dynamic-range neutron time-of-flight spectrometer located 13.4-m from the target chamber center (TCC) [19]. This diagnostic uses several microchannel-plate-based phototubes to increase the dynamic range required to measure the primary DT and DD signal in a single line of sight. The yield is inferred by fitting the recorded signal with a forward-fit approach using a relativistic model of the neutron distribution [20]. Cross-calibration of the neutron diagnostics with standard measurements on OMEGA give an uncertainty in the DT and DD yield of 5% and 9%, respectively [21,22]. In ignition-scalable implosions, the neutron yield is attenuated by the compressed fuel at peak neutron production (see Table I). To recover the fusion birth yield, a correction to the measured yields must be included as a function of the areal density from the compressed fuel. The primary D–T neutrons that elastically scatter off the cold-fuel distribution generate a “down-scattered” fraction ( $dsf$ ) that is directly proportional to the neutron-averaged areal density [23]. For this measurement, advanced detectors were developed to measure and calculate the number of neutrons that elastically scatter off the cold-fuel assembly [24]. Using the areal density, transmission factors ( $\eta_{DT}$  and  $\eta_{DD}$ ) for the neutrons from the two fusion reactions are calculated using the well-known total scattering cross sections. For typical areal densities achieved on OMEGA of up to 220 mg/cm<sup>2</sup>, a correction of up to 4% and 10% is needed for the DT and DD neutron yield, respectively. With the areal densities achieved on OMEGA, multiple scattering can be neglected, thereby providing an ideal platform to

study the effects of fuel-species separation in ignition-scalable implosions. By adding the uncertainty of the DT and DD yields, the attenuation of the yield from the compressed fuel and the reaction rate for both of the primary reactions in quadrature, an error of 10% for  $Y_{DT}/Y_{DD}$  ratio can be inferred.

As indicated earlier, it is important to know the ion temperature in the implosion and the fuel composition. The energy spread of the primary neutron distribution provides a good measure of the ion temperature characteristics of peak neutron production. If mass flow within the reaction region is present, this effect can lead to a broadening of peak distribution and an incorrect interpretation of ion temperature [20]. On OMEGA, several neutron time-of-flight detectors measure the width of the DT neutron spectrum temperature from various lines of sight around the target chamber [25]. The uncertainty in the inferred ion temperature is  $\pm 0.2$  keV for implosions between 2 keV and 5 keV. The ion temperature inferred from the width of the neutron spectrum in ignition-scalable implosions can vary up to  $\sim 1$  keV across the three different detectors. Simulations indicate that this variation in the temperature is caused by bulk fluid motion of the fusing plasma [26]. To minimize the effect of bulk motion, the minimum ion temperature will be used in this analysis as approximation to the thermal temperature. The histogram of the magnitude in the variation of the ion temperature can be evaluated to provide a standard deviation, which can be used as a measure of the uncertainty caused by bulk fluid motion. With the errors from the uncertainty of the ion temperature measurement and the standard deviation of the ion temperature variation, the inferred yield ratio has an uncertainty of less than 7%.

The observed reaction yield ratio is plotted as a function of the minimum ion temperature in Fig. 1 for each cryogenic shot on OMEGA (35 experimental campaigns with 120 implosions taken over a period of three years). The composition of the DT inventory in the assay volume is periodically measured on OMEGA to within an accuracy of 1.5%. In this case, the gas used to fill the targets was taken at various stages during the pressurization of the fuel so that the deuterium-to-tritium (D:T) concentration could be calculated. Over time, the tritium supply in the system gradually changes as a result of beta-decay of the hydrogen isotope. Figure 1 also shows the calculated ratios using the measured fuel fraction and the minimum ion temperature. The measured ratios show good agreement with the calculated ratios expected from the DT inventory and experimentally inferred ion temperatures. It should be noted that while the accuracy of the fuel composition in the both the assay volume and the pressurized system are well understood, an extrapolation of the fuel fraction is required of the gas composition during the fill process in the permeation cell that is used to fill cryogenic capsules. A project is underway to better characterize the fuel composition of the gas as it is sent into the permeation cell used to fill the capsules. Presently, this effect is known to change the composition between 3% and 5%. The calculated reaction yield ratios follow the form  $Y_{DT}/Y_{DD} \sim 2T_i^{0.4} (f_T/f_D)$  using the assumption that hydrodynamic models of an ICF implosion predict that the reactant density ratio ( $f_T/f_D$ ) is spatially and temporally constant during all phases. This indicates that additional effects that change this ratio or the volume over which each of the D–T and D–D reactions are produced do not significantly influence yields from the hot-spot stagnation. Pre-shot fuel fractions are measured during each fill process for every campaign. Variations in the yield ratio

measurements resulting from the fuel composition are reflected in Fig. 1 with the solid and dashed lines representing the initial and final measurement, respectively, before the inventory underwent a scheduled refinement.

The measured D–T and D–D yield ratios and the ion temperature are used to instead infer a fuel fraction ( $f_D$  and  $f_T$ ) for each of these shots. The measured fuel fraction is compared against values inferred from nuclear measurements in Fig. 2. The average of the ratio of the inferred fuel fraction from the nuclear measurement over the composition obtained from the permeation cell is 1.07 with a standard deviation of 0.09. Although error on the mean is small with 1% for 120 implosions used for this study, given the 10% systematic error on the  $Y_{DT}/Y_{DD}$  ratio, both measurements of the fuel fractions are consistent within the experimental uncertainties.

In summary, nuclear measurements of the D–T to D–D yield ratio from OMEGA cryogenic implosions scale predictably with the measured composition of the pre-shot fuel and inferred ion temperatures within the experimental uncertainties. These observations indicate that multifluid effects that may take place during the shock phase of the implosion (and potentially influence species profiles in the compressing target) do not persist into the subsequent compression phase of the implosion. A plausible explanation for this rests on the composition of the target; the shell is also deuterium–tritium fuel. During the deceleration phase of cryogenic DT implosions, the fuel from the inner DT wall is ablated into the hot spot. Simulations indicate that nearly  $5\times$  the mass of the neutron-emitting region is from the ablation of the cold DT shell. Therefore, the energetic ions that may be lost because of their long mean free paths earlier in the implosion return to the hot spot during peak neutron production, leading to an unchanged fusion yield

ratio. These observations indicate that multifluid effects have an insignificant influence on the yield ratio in ignition-scalable cryogenic implosions.

The largest contribution to the uncertainty in the yield ratio measurement is caused by the absolute calibration of the DD yield diagnostic used to cross-calibrate the high-dynamic-range diagnostic for each cryogenic campaign. Future experiments will improve the accuracy of the calibrated DD yield diagnostic and decrease the absolute uncertainty from 9% to 5%. These experiments will reduce the  $Y_{DT}/Y_{DD}$  ratio as measured by the high-dynamic-range diagnostic down to 7% which, in turn, will improve the accuracy of the inferred fuel fractions obtained from this measurement. Presently, there is no measurement available of the true temperature of the plasma, which is very important for this measurement. Several projects are being considered that will provide a true thermal temperature that is not influenced by the bulk fluid motion of the plasma.

## **ACKNOWLEDGEMENT**

The authors thank the OMEGA operations crew for their help in executing these experiments. This material is based upon work supported by the Department of Energy National Nuclear Security Administration under Award Number DE-NA0001944, the University of Rochester, and the New York State Energy Research and Development Authority.

This report was prepared as an account of work sponsored by an agency of the U.S. Government. Neither the U.S. Government nor any agency thereof, nor any of their employees, makes any warranty, express or implied, or assumes any legal liability or responsibility for the accuracy, completeness, or usefulness of any information,

apparatus, product, or process disclosed, or represents that its use would not infringe privately owned rights. Reference herein to any specific commercial product, process, or service by trade name, trademark, manufacturer, or otherwise does not necessarily constitute or imply its endorsement, recommendation, or favoring by the U.S. Government or any agency thereof. The views and opinions of authors expressed herein do not necessarily state or reflect those of the U.S. Government or any agency thereof.

## REFERENCES

1. H. Brysk, *Plasma Phys.* **15**, 611 (1973).
2. D. T. Casey *et al.*, *Phys. Rev. Lett.* **108**, 075002 (2012).
3. M. J. Rosenberg *et al.*, *Phys. Plasmas* **21**, 122712 (2014).
4. H. G. Rinderknecht *et al.*, *Phys. Rev. Lett.* **114**, 025001 (2014).
5. D. B. Henderson, *Phys. Rev. Lett.* **33**, 1142 (1974).
6. V. N. Goncharov *et al.*, *Phys. Plasmas* **21**, 056315 (2014).
7. J. Delettrez, R. Epstein, M. C. Richardson, P. A. Jaanimagi, and B. L. Henke, *Phys. Rev. A* **36**, 3926 (1987).
8. S. P. Regan *et al.*, *Phys. Rev. Lett.* **117**, 025001 (2016).
9. C. D. Zhou and R. Betti, *Phys. Plasmas* **14**, 072703 (2007).
10. W. T. Shmayda, M. D. Wittman, R. F. Earley, J. L. Reid, and N. P. Redden, *Fusion Eng. Des.* **109–111**, Part A, 128 (2016).
11. I. V. Igumenshchev *et al.*, *Phys. Plasmas* **19**, 056314 (2012).
12. V. N. Goncharov *et al.*, *Phys. Plasmas* **13**, 012702 (2006).
13. I. V. Igumenshchev *et al.*, *Phys. Plasmas* **23**, 052702 (2016).
14. S. X. Hu, V. N. Goncharov, P. B. Radha, J. A. Marozas, S. Skupsky, T. R. Boehly, T. C. Sangster, D. D. Meyerhofer, and R. L. McCrory, *Phys. Plasmas* **17**, 102706 (2010).
15. I. V. Igumenshchev, V. N. Goncharov, W. T. Shmayda, D. R. Harding, T. C. Sangster, and D. D. Meyerhofer, *Phys. Plasmas* **20**, 082703 (2013).
16. P. Amendt, O. L. Landen, H. F. Robey, C. K. Li, and R. D. Petrasso, *Phys. Rev. Lett.* **105**, 115005 (2010).

17. G. Kagan and X.-Z. Tang, *Phys. Lett. A* **378**, 1531 (2014).
18. H.-S. Bosch and G. M. Hale, *Nucl. Fusion* **32**, 611 (1992).
19. C. J. Forrest, V. Yu. Glebov, V. N. Goncharov, J. P. Knauer, P. B. Radha, S. P. Regan, M. H. Romanofsky, T. C. Sangster, M. J. Shoup, and C. Stoeckl, *Rev. Sci. Instrum.* **87**, 11D814 (2016).
20. L. Ballabio, J. Källne, and G. Gorini, *Nucl. Fusion* **38**, 1723 (1998).
21. O. Landoas, V. Yu. Glebov, B. Rossé, M. Briat, L. Disdier, T. C. Sangster, T. Duffy, J. G. Marmouget, C. Varignon, X. Ledoux et al., *Rev. Sci. Instrum.* **82**, 073501 (2011).
22. C. Waugh, M.S. thesis, Massachusetts Institute of Technology, 2014.
23. J. A. Frenje *et al.*, *Phys. Rev. Lett.* **107**, 122502 (2011).
24. C. J. Forrest *et al.*, *Rev. Sci. Instrum.* **83**, 10D919 (2012).
25. V. Yu. Glebov *et al.*, *Rev. Sci. Instrum.* **81**, 10D325 (2010).
26. T. J. Murphy, *Phys. Plasmas* **21**, 072701 (2014).

## Figure captions

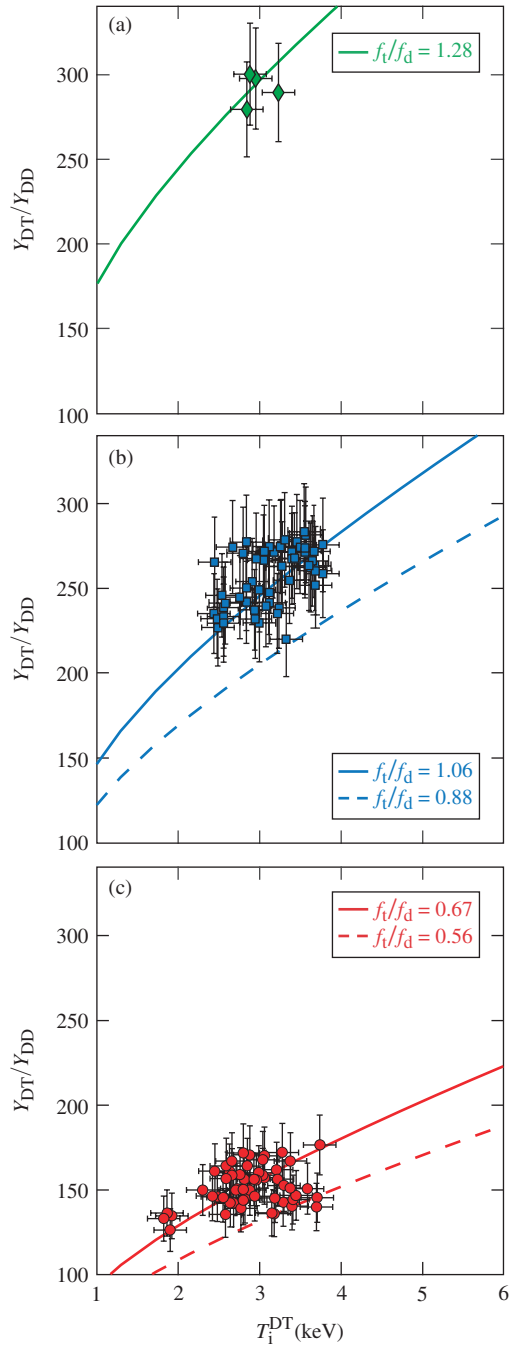
FIG. 1. With each cryogenic implosion, the  $Y_{DT}/Y_{DD}$  yield ratio is plotted with the minimum DT neutron average ion temperature. The T:D fuel fraction used to fill the cryogenic targets varied between  $f_T/f_D \sim 0.58$  (a) and  $f_T/f_D \sim 1$  (b) for the majority of the cryogenic targets. A single campaign (c) had a fill fraction of  $f_T/f_D \sim 1.28$ . The solid line represents the initial measurement of fuel inventory and the dashed line shows how much the fuel has changed over time due to decay of tritium. The hydrogen concentration does not contribute to the fusion yield and is not included in this analysis.

FIG. 2. The measured fuel fraction determined at the fill station (assay measurement) is compared with the values inferred from the nuclear measurements over a three-year period. The changes in the fuel fraction used to fill the targets is clearly visible between  $f_D/f_D \sim 0.6$  and  $f_T/f_D \sim 1$ . A single campaign with four implosions had a fill fraction of  $f_T/f_D \sim 1.28$ .

## TABLES

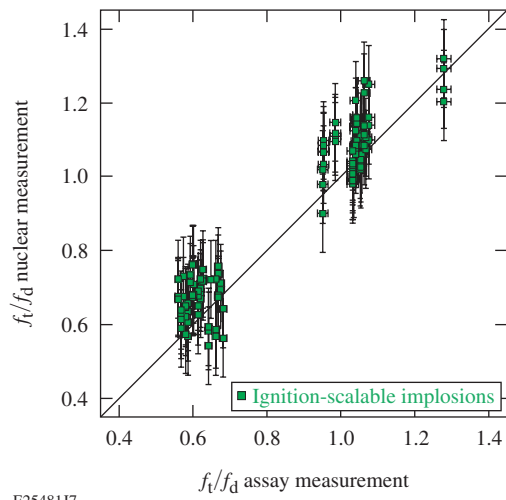
Table I: Calculated implosion parameters for various plasma conditions ranging from a highly kinetic exploding pusher (in the shock phase in the vapor) to a strongly hydrodynamic-like plasma regime (cold-fuel layer in the shock or compression phase).

Implosion Type	$\rho$ (g/cm <sup>3</sup> )	$T_i$ (keV)	$\lambda_{ii}$ ( $\mu\text{m}$ )	$R_{\text{shell}}$ ( $\mu\text{m}$ )
Exploding pusher				
Shock phase	0.03	10	400	100
Cryogenic implosions				
Shock phase: vapor	0.1	8	80	100
Shock phase: cold-fuel layer	6.0	0.02	0.0002	$\Delta R_{\text{shell}} \sim 10$
Compression phase	20.0	3	0.08	25



E25147J7

Figure 1 LX14815 20JAN2017



E25481J7